Published in final edited form as:
Mod Phys Lett B. 2014 December 10; 28(30): . doi:10.1142/S0217984914300154.

Understanding dynamic changes in live cell adhesion with neutron reflectometry

ANN JUNGHANS,
MPA-CINT/Lujan Neutron Scattering Center, Los Alamos Neutron Science Center, Los Alamos National Laboratory, Los Alamos, New Mexico, 87545, USA

MARY JO WALTMAN,
Biosciences Division, Bioenergy and Biome Sciences, Los Alamos National Laboratory, Los Alamos, New Mexico, 87545, USA

HILLARY L. SMITH,
Department of Applied Physics and Materials Science, California Institute of Technology, Pasadena, CA 91125, USA

LUKA POCIVAVSEK,
Department of Surgery, University of Pittsburgh Medical Center, 200 Lothrop St, Pittsburgh, PA 15213, USA

NOUREDDINE ZEBDA,
NDA Analytics, Woolley Road, Huntingdon, Cambridgeshire, PE28 4HS, UK

KONSTANTIN BIRUKOV,
Lung Injury Center, Department of Medicine, The University of Chicag; 5841 S. Maryland Ave., Chicago, IL 60637, USA

MARIANO VIAPIANO, and
Department of Neurosurgery, Brigham and Women's Hospital and Harvard Medical School 4 Blackfan Circle, Boston, MA 02115, USA

JAROSLAW MAJEWSKI
MPA-CINT/Lujan Neutron Scattering Center, Los Alamos Neutron Science Center, Los Alamos National Laboratory, Los Alamos, New Mexico, 87545, USA

ANN JUNGHANS: annjunghans@lanl.gov; MARY JO WALTMAN: waltman@lanl.gov; HILLARY L. SMITH: HLS@caltech.edu; LUKA POCIVAVSEK: pocivavsekl@upmc.edu; NOUREDDINE ZEBDA: Noureddine.Zebda@NDA-Analytics.com; KONSTANTIN BIRUKOV: kbirukov@medicine.bsd.uchicago.edu; MARIANO VIAPIANO: mviapiano@partners.org; JAROSLAW MAJEWSKI: jarek@lanl.gov

Abstract

Neutron reflectometry (NR) was used to examine various live cells adhesion to quartz substrates under different environmental conditions, including flow stress. To the best of our knowledge, these measurements represent the first successful visualization and quantization of the interface between live cells and a substrate with sub-nanometer resolution.

In our first experiments, we examined live mouse fibroblast cells as opposed to past experiments using supported lipids, proteins, or peptide layers with no associated cells. We continued the NR studies of cell adhesion by investigating endothelial monolayers and glioblastoma cells under

dynamic flow conditions. We demonstrated that neutron reflectometry is a powerful tool to study the strength of cellular layer adhesion in living tissues, which is a key factor in understanding the physiology of cell interactions and conditions leading to abnormal or disease circumstances. Continuative measurements, such as investigating changes in tumor cell – surface contact of various glioblastomas, could impact advancements in tumor treatments. In principle, this can help us to identify changes that correlate with tumor invasiveness. Pursuit of these studies can have significant medical impact on the understanding of complex biological problems and their effective treatment, *e.g.* for the development of targeted anti-invasive therapies.

Keywords

cells; endothelial monolayer; glioblastomas; adhesion; shear stress; neutron scattering

1. Overview

Adhesion of cells to an underlying substrate plays a crucial role in physiology and disease[1–3] and has been investigated with great interest for several decades. Some of the measurement techniques used are interference reflection microscopy (IRM),[4–8] fluorescence interference contrast microscopy (FLIC),[9–11] total internal reflection fluorescence microscopy (TIRFM),[12–16] and surface plasmon resonance microscopy (SPRM).[17,18] In the current studies, we report on sub-nanometer resolution measurements of the adhesion layer of different live cells on quartz by neutron reflectometry (NR). Due to the penetrability of neutrons, this technique is commonly used to probe thin films with thicknesses of 5–5000 Å at various buried interfaces. Over the past two decades, the method has evolved to become a key tool in the characterization of biological and biomimetic thin films.[19,20] Typically, NR measurements are performed on homogeneous model systems, such as phospholipid monolayers at the air-liquid interface,[21] pure and hybrid phospholipid bilayers on silicon and quartz substrates,[22–25] and phospholipid bilayers on novel support systems designed to more closely mimic biological membranes.[26,27]

Because live cell adhesion to a solid substrate is complex and intrinsically non-homogeneous over the large area studied (approx. 10 cm^2), these studies represent a radical departure from the typical systems measured *via* NR. Such measurements will establish a precedent for *in situ* NR measurements of complex biological systems much more relevant than their surrogate counterparts. By expanding our research to two exemplary systems of huge medical importance (*i*) large endothelial surfaces that control the flow of fluid and molecules throughout tissues and (*ii*) cancerous cells that loosen their attachments to give rise to distant metastases, we demonstrate that neutron reflectometry can impact the understanding of complex biological systems under dynamic (flow) conditions and lead to future effective treatment, *e.g.* the development of targeted anti-invasive therapies.

2. Methods

NR is an excellent tool to study the structure of living tissue at the solid-liquid interface *in situ*. Neutrons are highly sensitive to the scattering contrast between hydrogenated and deuterated materials. An example is neutron scattering from hydrogenated alkyl tails of

phospholipid bilayers (which are not capable of an isotopic exchange) measured in a deuterated subphase (D_2O). During a NR experiment, neutrons penetrate through the support substrate (*e. g.* quartz wafer), which is in contact with the liquid subphase and are scattered from the structure of interest, for example cells deposited on the substrate, at a small angle, θ (Figure 1 *c*). The ratio of elastically and specularly scattered neutrons to incident neutrons is measured. This ratio is defined as the reflectivity, *R*, and is measured as a function of the momentum transfer vector, Q_z, where $Q_z=4\pi\sin[\theta]\lambda^{-1}$ where λ is the neutron wavelength. In our case, the different values of the Q_z vector are obtained by both λ and θ variation. NR measurements were performed at the Surface Profile Analysis Reflectometer (SPEAR) beam line at the Los Alamos Lujan Neutron Scattering Center.[28] The neutron beam is produced from a spallation source and moderated by liquid H_2. The different λ are discriminated by a time-of-flight (ToF) position-sensitive detector. The range of λ utilized in this work was from 4.5 to 16 Å. The reflectivity data is plotted as $R/R_{Fresnel}$ versus the perpendicular scattering vector Q_z, thus accounting for the Q_z^{-4} decrease of the reflectivity due to Fresnel's law.[29]

Analysis of the specular reflectivity *vs.* Q_z enables development of the scattering length density (SLD) distribution along normal to the sample surface.[30] SLD is a function of chemical composition and density of the material. The SLD profile obtained from NR measurements provides structural information at a very high spatial resolution (<10 Å). Specifications of NR measurements and modeling of the data have been detailed elsewhere.[28,30] In our studies, modeling of the SLD distributions was performed using an open-source reflectivity package, MOTOFIT, which runs in the IGOR Pro environment.[31] MOTOFIT approximates the continuous SLD function by the number of layers with constant SLDs. An error function centered between two adjacent interfaces is used to address the interfacial roughness. A theoretical reflectometry curve can be calculated using Abeles matrix formalism. Both Genetic optimization and Levenberg–Marquardt nonlinear least-square methods were employed to obtain the best fits with the lowest χ^2 values and structurally meaningful parameters for the NR data. To model the NR data, the SLD value of the quartz substrate was fixed to 4.18×10^{-6} Å^{-2} in all cases. In all experimental data presented, D_2O based buffers were used as the subphase. From our experience we know that the cells can survive up to 6 hours in such conditions without visible changes in the cells' viability. Using D_2O based subphases was necessary to obtain sufficient scattering contrast. The main source of such contrast is due to the neutron scattering differences between the hydrogenated lipid membrane facing the quartz substrate (low SLD) and the D_2O hydrated environment (high SLDs).

If any of the studied systems changes, *e.g.* the adhesion of the cells to the quartz substrate, the scattering length density distribution will change. This change in SLD distribution will be immediately apparent in the scattering from the system. For example, a rearrangement in the density or chemical composition of the extracellular matrix upon shear can be observed as a change in scattering reflectivity. A modification of the thickness of this layer would result in altered fringe spacings. This is illustrated in Figure 2 a, b where the density, hydration and interfacial roughness of all components (protein rich extracellular matrix, ECM between the solid substrate and the cell's lipid membrane, cell lipid membrane, and

intracellular matrix, ICM) was kept constant while the distance between the solid substrate and the lipid membrane was varied. Figure 2 *c*, *d* represents another case where the thickness and interfacial roughness of all the scattering components was kept constant but the amount of proteins in the extracellular region was allowed to increase, simulating the secretion of adhesive components anchoring the cells to the quartz substrate. This case would be visible in a decrease of the SLD due to more hydrogen in the ECM layer.

Measurements were conducted on cell monolayers grown on a flat surface of monocrystalline quartz. Cell monolayers were perfused with culture medium at controlled conditions to reach a laminar shear stress level of 1.5 Pa or left static, as previously described.[32]

All shear experiments were conducted in a custom-built neutron scattering solid-liquid interface cell (Figure 1). The measurement cell consists of two main parts: a base made of Macor ceramic and a monocrystalline quartz wafer (Figure 1 *c*). Cells were grown on the bottom of the quartz disc (shown schematically in Figure 1 *d*). The Macor part is equipped with a fluid inlet, outlet and an O-ring trench. The O-ring separates the ceramic base from the quartz crystal. Both parts are kept together by a clamping mechanism. The distance between the ceramic base and the crystal is approximately 0.2 mm and can be regulated by the tension on the clamping system. The geometry of the cell's inlets and outlets are designed to allow a laminar flow of liquid between the ceramic and the quartz. The laminarity of the flow was modeled by hydrodynamic simulations using commercial software (Figure 1 *b*). The width and the length of the cell over which the flow can be considered laminar is 35×50 mm^2 and is coinciding with the size of the footprint of the neutron beam. A pulse-less gear pump was used to produce the flow required for the experiments.

The preparation of cells and experimental procedures has been explained in detail in previous publications. [32,33]

3. Results

3.1 Mouse Fibroblast Cell Adhesion

In a groundbreaking proof-of-principle experiment that represents a significant advancement towards employing neutron reflectometry to measure complex biological samples, we examined live mouse fibroblast cells adherent on a quartz substrate in a deuterated phosphate-buffered saline environment at room temperature.[32] This series of experiments represents, to our knowledge, the first successful visualization and quantization of the interface between live cells and a substrate using NR, since we observed a clear signal attributable to live HK-03 mouse fibroblast cells, confirmed by comparison with samples of pure medium.

Figure 3 *a* shows NR measurements and best-fit models and Figure 3 *b* the corresponding SLD profiles. The approx. 80 Å dip in SLD (to ~ 1.8×10^{-6} $Å^{-2}$) centered at 400 Å from the quartz substrate represents the hydrocarbon tails of the cell lipid membrane. The thickness of the hydrocarbon component of a pure phospholipid bilayer is typically ~40 Å, the length

of two hydrophobic tails. A membrane region twice this thick suggests that the membranes of the adhering cells are not organized as a homogeneous plane uniformly spaced from the quartz substrate. Instead, the membrane is likely either undulating or non-homogeneous distributed due to the surface topography of the underlying media and adherence proteins. An alternative explanation is that the neutron scattering averages over several neighboring cells (in the coherent volume of the neutron beam, which is typically ~1×100 μm^2) varied in their distance from the solid substrate. Immediately at the quartz interface is a thick layer of proteins. The SLD in this region is different from that for the pure media sample. Though the exact composition of this region is unclear, it is important to recognize the differences between samples with and without cells, 0–360 Å from the quartz substrate. This difference may provide evidence that the cells are indeed secreting proteins to adhere to the substrate, changing the composition of the cell-substrate interface. The interior of the cell region, 440–600 Å from the substrate, contains some hydrogen-rich material in the vicinity of the membrane, which transitions to the SLD of pure dPBS over ~150 Å. One might expect to see the other leaflet of the cell membrane visible at a much greater distance from the quartz substrate. However, using SPEAR, the largest resolvable feature measurable for an extremely homogeneous sample is approx. 3000 Å. Based on the cell surface area calculations given above (660 μm^2 per cell) and the mean volume of a single HK-03 cell (1870 μm^3), the thickness of a cell adherent to the substrate can be estimated at 2.8 μm. This is ~ 10 times the distance from the quartz surface over which SPEAR measurements can be made.

Samples with high and low cell surface density were prepared. In Figure 3, NR data from a representative low-density sample is depicted along with data from a high cell surface density. A comparison of the high and low cell surface density NR profiles shows that the overall shape of the scattering curve is preserved, indicating that the length scales are similar between the two samples. However, the overall reflected intensity is lower for the sample with lower cell surface density. The SLD profile for the low cell density data was generated by model-dependent fitting with the intent to mimic the one obtained for higher cell surface density. As shown in Figure 3 *b*, the length scales of the two systems are almost identical, but in the lower cell surface density case, the overall is increased, suggesting a larger volume fraction of dPBS at lower cell surface density.

To further confirm the accuracy of our NR measurements on live cells, we measured the effects of distilled water and trypsin on our cell samples. Both distilled water and trypsin are expected to disturb the cell monolayer on the substrate. After exposure to distilled water, the SLD profile (data not shown) showed a featureless transition from the SLD of the quartz substrate to the SLD of the bulk dPBS subphase, indicating that the distilled water effectively removed the cells from the substrate. Similarly in the second case, the disappearance of features in the NR profile after the introduction of trypsin indicates that the cells are no longer adherent (data not shown).

The above measurements of live cells with NR represent an ability to extract information from a system as complicated as live cells at angstrom resolution not accessible by optical methods. As will be demonstrated below, probing the detailed structure and biophysics of

cell attachment *in situ* and their response to the shear stress generated by flow, can have significant medical importance.

3.2 Tuning Endothelial Adhesion with Temperature and Fluid Shear Stress

Endothelial cells (EC) are the master gatekeepers of the cardiovascular system. Interruption of endothelial function is linked to complex diseases such as arterial plaque build-up and acute respiratory distress. Critical to proper function within the endothelium is mechanical stimulation from shear stress. Adhesion to the underlying extracellular matrix (ECM) is a crucial component of how endothelial cells sense and transmit mechanical signals. In this study, we used neutron reflectometry to measure for the first time the nanoscopic structure of confluent endothelial monolayer interfaces.[33] The linkage between blood flow, the endothelial monolayers adhesiveness to the basal lamina and its ability to function as the gatekeeper of vascular permeability is clearly established; moreover, with examples ranging from acute respiratory distress syndrome to atherosclerosis, there is tremendous clinical importance in understanding this relationship.[34–38] We used confluent monolayers of human pulmonary arterial endothelial cells grown on single-crystal quartz blocks at 25°C and 37°C, under static conditions or a laminar fluid shear stress τ=1.5 Pa (equivalent to arterial conditions).

Figure 4 shows the neutron reflectivity data and derived scattering length density profiles at the four conditions studied. The basal lamina is spectroscopically defined as the volume element starting at the quartz/liquid interface and ending at the well-characterized lipid bilayer signature of the plasma membrane. Endothelial cells generate their own extracellular matrix, called basal lamina, making it possible to grow monolayers on inert surfaces like quartz without prior exogenous deposition of protein layers.[1,39] A key component in the structure, mechanical coupling, and stability of endothelial basement membranes is type IV collagen.[39–41] Under all four conditions, the composition of the basal lamina indicates a well hydrated (D_2O content ~ 40%) protein network, which proves to be insensitive to temperature or shear stress. However, basal lamina thickness *l* proves to be highly sensitive to these perturbation fields. Under static conditions (Figure 4 b, c), we observe a near tripling of *l* as the temperature is raised from 25°C to 37°C ($l^{st}_{25^\circ C} \approx 200\text{Å}, l^{st}_{37^\circ C} \approx 600\text{Å}$). Interestingly, shear stress has the opposite effect at the two temperatures (Figure 4 d, e), causing cell separation at 25°C while inducing movement closer to the substrate at physiologic temperature ($l^{ss}_{25^\circ C} \approx 700\text{Å}, l^{ss}_{37^\circ C} \approx 200\text{Å}$).

During the NR studies, the off-specular (or diffuse) scattering signal was also recorded. The scattered neutron intensity as a function of the in-plane components of the momentum transfer vector provides information about fluctuations along the surface of the studied system. Figure 5 shows diffuse neutron reflectivity data for the studied system at 37°C. The high intensity peak at $p_i p_f = 0$ corresponds to the specular reflection. Standard reflectivity theory states that the intensity distribution of the off-specular scattering ($p_i - p_f \neq 0$) directly corresponds to the degree of interfacial fluctuations.[42] Our data shows that the off-specular peak enlarges with increasing temperature under static conditions (data for 25°C not shown) while it substantially decreases with shear flow for both temperatures. Temperature, as expected, increases interfacial thermal fluctuations. Shear stress acts in a reverse manner by

placing the cells (and therefore their lipid membranes) under tension, thereby suppressing fluctuations and decreasing the off-specular intensity.

Shear stress plays an important and growingly recognized role in endothelial biology. [2,3,35,36,38,43] Our study is the first to provide a direct measure of endothelial monolayer adhesion under physiologic shear stress conditions. Biomechanical analysis of endothelial stress distributions[33] predicts that to avoid catastrophic endothelial delamination, part of the fluid shear stress τ is transmitted to the basal lamina.[2,3] Thermodynamically, luminal flow does work (proportional to the product of shear stress and cell size) against the static adhesion energy. The de-attachment of endothelial monolayers under flow at 25°C is in agreement with this thermodynamic argument. At 25°C, most active biology is suppressed and the endothelial monolayer responds more like a soft matter physical system as seen above. At physiologic temperatures, however, the full richness of cell biology is available to the system.

This can, for example, be shown by Trans-endothelial Electrical Resistance (TER) measurements (Figure 6). The sharp permeability increase to vasoactive agonist thrombin seen at 37°C is abolished in EC cultured at 25°C. This method has been demonstrated to be a highly sensitive biophysical assay that indicates the state of cell shape and focal adhesion.[44,45] For those experiments, endothelial cells were grown to confluence in polycarbonate wells containing evaporated gold microelectrodes (surface area, 10^{-3} cm^2) in series with a large gold counter electrode (1 cm^2) connected to a phase-sensitive lock-in amplifier. The size of the small gold electrode is critical so that the impedance resulting from the presence of cells on the electrode will predominate over the resistance of the medium. Measurements of trans-monolayer electrical resistance were performed using an electrical cell-substrate impedance sensing system (Applied BioPhysics Inc., New York, USA). Briefly, current was applied across the electrodes by a 4,000-Hz AC voltage source with amplitude of 1 V in series with a 1 M resistance to approximate a constant current source 1 μA. The in-phase and out-of-phase voltages between the electrodes were monitored in real time with the lock-in amplifier and subsequently converted to scalar measurements of trans-monolayer impedance, of which resistance was the primary focus. The culture medium was replaced to basal media containing 2%FBS; TER was monitored for steady state achieved and started again for 30 minutes to establish a baseline resistance (R_0).

Shear stress causes major redistribution of proteins involved in cell-cell (adherens junction complexes) and cell-substrate adhesion (focal adhesions). Even on relatively short biological time scales (4 h) relevant to the time scale of our neutron experiments, adherens junctions (β-catenin stain) and focal adhesions (paxillin stain) undergo localization to the cortical rim of endothelial cells.[33] This localization of adhesion proteins is postulated to promote linkage between the actin skeleton and extracellular matrix, forming enhanced adhesion zones.[35] Bruinsma *et al*.[46] and Sackmann and Bruinsma[47] explored the theoretical effect of specific adhesion binding proteins on single cell adhesion potentials. They concluded that adhesion molecules change the interfacial energy landscape allowing access to strong adhesion zones rich in specific adhesion molecules. Our measurement shows that this biological effect may indeed be at work in endothelial monolayers as well. Shear stress at 37°C causes localization of specific proteins which may alter the adhesion potential in favor of overall increased

adhesion as measured with neutrons. This biological response competes against the purely physical effects of shear flow observed at 25°C and the increased repulsive potential of the basal lamina at higher temperatures.

Mechanical forces play an intricate role in biological systems from the tissue and organ level down to individual cells and even proteins.[48–50] Most existing work in endothelial mechano-biology has focused on single cells and even single molecules and protein complexes. Yet the collective behavior of the monolayer of cells has been less well explored. It is clear, however, that endothelial cells make strong lateral connections between each other and that these connections change as a function of mechanical stress. The above results are the first successfully completed neutron reflectometry experiments on living human endothelial cells under fluid mechanical shear stress that provide valuable insight on the boundary layer dynamics of complex bio-medical systems. These studies could lead to advances in the treatment of atherosclerosis and other disorders associated with the cardiovascular system.

3.3 Behavior of extracellular matrix of glioblastoma under shear

Using endothelial monolayers, we showed that physical models of soft-adhesion can describe large scale tissue adhesion, which broadens their scope of application far beyond the single cell realm. The strength of neutron reflectometry is its non-pertubative nature, the ability to probe large surface areas of buried interfaces with nanometer resolution, and the possibility of scattering contrast manipulation *via* the isotopic substitutions. That allows us to probe details of the cell-substrate interface that are not accessible with any other standard techniques. Such capabilities can also be employed to obtain better insight into the mechanisms of cell adhesion and cell-surface properties of clinically relevant systems such as cancerous cells. This can provide new ways to address biomedical challenges connected with the behavior of these cells. Therefore we extended the above investigations to study the adhesion of several types of brain tumor cells (Table 1) under static and flow shear conditions.

Gliomas are the most common and aggressive type of tumors that originate in the brain[51] and one of the solid cancer types with poor prognosis.[52] The most common type of glioma, known as glioblastoma (GBM), is highly resistant to conventional chemo- and radio-therapy and results in median survival of less than 14 months after diagnosis.[53] In addition to being isolated within the central nervous system, which makes them difficult to reach with conventional therapies, a major escape mechanism that contributes to the poor outcome of GBMs is the highly invasive nature of the tumor cells.[52] Improved understanding of the molecular mechanisms that facilitate GBM cell adhesion to neural tissue structures and promote brain invasion is critical to increase the long-term efficacy of current therapies.[54,55]

Local invasion of GBM cells appears to involve only restricted degradation of the surrounding stroma.[56,57] Instead, invasion is mostly facilitated by mechanisms of cell adhesion and rapid changes in the volume of the cell body as the tumor cell maneuvers through intercellular spaces.[56,58] Adhesion mechanisms are facilitated by adhesion receptors (*e.g.*, integrins) and changes in the composition of a pro-adhesive extracellular matrix (ECM) surrounding the invasive cells.[57,59–61] In addition, GBM cells at the border of the tumor are exposed to local shear stress arising from the increased cell density, rigidity, and

fluid retention inside the tumor, which generates positive outward pressure.[62,63] While the role of shear stress in intracranial GBMs is not yet defined, recent work has shown that some models of shear stress can modulate metalloprotease expression and GBM cell invasion *in vitro*.[64]

In our study, we analyzed the properties of three GBM cell lines (Table I) that have been previously characterized by their migratory properties *in vitro* and invasive properties when they are implanted intracranially in athymic mice.[65] We hypothesized that the different adherent and invasive properties of these well-characterized cells could be supported by different cell surface properties that would be revealed with the sub-nanometer resolution of neutron reflectivity. To test this hypothesis, we analyzed the interactions of the GBM cells with untreated quartz substrate by culturing them at 37°C in DMEM containing 10% calf serum and D_2O, in static and shear conditions (Figure 7). All NR experiments were performed at 37°C.

The first important difference we observed in the cells measured in static conditions is noticeable in the SLD profile for non-invasive U251 cells, which show a thicker glycocalyx/ ECM layer. Such surrounding layer contrasts them from the invasive CNS1 and GL261 cells (Figure 7). This “adhesion layer” is largely composed of hyaluronic acid (HA) and associated proteoglycans,[60] which are more abundant around GBM cells than normal glial cells.[66,67] A thick HA coating can promote cell adhesion but limit GBM invasion *in vivo* if not degraded by tumor-produced hyaluronidases.[68] Therefore, from our SLD analysis we hypothesize that U251 cells may likely have higher production of HA than the rodent GBM cells, which could contribute both to their non-fibroblastic morphology and limited invasive ability.

More striking differences were observed under shear conditions, when compared to previous measurements on endothelial cells. Upon shear, the thickness of the glycocalyx/ ECM layer that attaches the GBM cells to the quartz substrate did not decrease as in the case of endothelial cells. Both CNS1 and U251 cells retained an adhesion layer of approximately the same thickness when subjected to shear, while the thickness of this layer even increased in the case of GL261 cells (Figure 8). This increase in the thickness of the extracellular layer was a striking contrast with our previous observations in endothelial cell monolayers: The thinner extracellular layer in endothelial cells exposed to shear increases their adhesion to the substrate and may reflect their specialization to maintain a barrier between circulating fluids and tissue. In contrast, the sustained or increased thickness of this layer in GBM cells suggests reduced substrate adhesion and may reflect a unique property of individual migratory cells that allows them to retain motility.

In all GBM cases studied, we observed a decrease in SLD in response to shear stress, indicating a denser (more protein rich) glycocalyx/ECM layer. Unlike in the case of the endothelial cells at 37°C this was not caused by “compaction” of the ECM due to closer attachment to the substrate but likely due to ECM-remodeling mechanisms. We have previously shown that overexpression of the major HA-synthase in glioma cells (*HAS2* gene) can cause an increase of several microns in the thickness of the surrounding ECM within 24 hours (Figure 9).[69] Increased synthesis of HA (which retains water and ions) and

secreted proteoglycans, plus rapid changes in total cellular volume, could explain in part the rapid increase in thickness in response to shear. Future use of HA and CSPG synthesis inhibitors (4-methylumbelliferone and beta-D-xyloside, respectively) will help define the contribution of these molecules to the observed phenomenon. Interestingly, comparison of these results with the prior results of U251 cells under static conditions leads us to hypothesize that shear may not only increase the production of HA in GL261 cells but could also correlate with a reduction in their invasive ability. This could explain the limited dispersion of these cells out of the tumor core in the brain.[70]

In summary, the presented results reveal differences in the thickness and composition of adhesion layer of different GBM cells in the static conditions as well as changes of this layer when the cells were subjected to shear stress. These differences may be specifically associated with mechanisms of brain tumor invasion. Further studies of these cells by neutron reflectometry under a variety of conditions (biological substrates, flow, drug treatments) will perhaps allow us to determine conditions triggering changes in the composition, density and thickness of the bio-material at the cell surface (in our case, the ECM layer). This, in turn, can help to identify changes that correlate with increased or decreased tumor invasiveness. Pursuit of those studies can have significant medical impact for the development of targeted anti-invasive therapies for GBM.

4. Outlook

We have described a series of experiments that represent, to our knowledge, the first successful visualization and quantization of the interface between live cells and a substrate using neutron reflectometry in static and dynamic conditions. In our view, the measurements of live cells with NR may represent a significant new direction for the study of highly complex biological systems.

Historically, NR measurements have been limited to homogeneous model systems. The ability to extract information from a system as complicated as live cells will enable many similar measurements to be made in the future. A major benefit of our method is that NR measurements can be made on viable cells in liquid medium. This configuration makes it possible to examine the attachment region of cells under a variety of conditions, such as different compositions of the subphase and extracellular matrix or biochemical or genetic alteration of the cellular expression of attachment molecules. As we show for the exemplary systems, NR measurements of viable, attached cells can be a powerful tool of probing the detailed structure and biophysical processes connected with the cell adhesion *in situ.* Such measurements can be performed with minimum measurement disturbance and can have significant medical implications. The presented work not only develops a new tool to study adhesion in highly complex living systems but also provides unique structural data on their behavior in shear stress conditions. We observed that at 37°C shear stress decreases the thickness of the adhesion layer in healthy endothelial monolayers, but can lead to the opposite effect in cancerous glioblastoma cell lines.

In conclusion, we hope the reader appreciates the opportunities neutron reflectometry provides for understanding biomedical questions and to catalyze innovative studies.

Acknowledgments

This work benefited from the use of the Lujan Neutron Scattering Center at LANSCE funded by the DOE Office of Basic Energy Sciences and Los Alamos National Laboratory under DOE Contract DE-AC52-06NA25396.

References

1. Birukov KG, Leitinger N, Bochkov VN, Garcia JGN. Microvascular Research. 2004; 67:18. [PubMed: 14709399]
2. Fung, YC. Biomechanics: Mechanical Properties of Living Tissues. 2. Springer-Verlag; New York: 1993.
3. Fung YC, Liu SQ. J Biomech Eng. 1993; 115:1. [PubMed: 8445886]
4. Curtis AS. J Cell Biol. 1964; 20:199. [PubMed: 14126869]
5. Gingell D, Todd I. Biophys J. 1979; 26:507. [PubMed: 262429]
6. Izzard CS, Lochner LR. J Cell Sci. 1976; 21:129. [PubMed: 932106]
7. Schindl M, Wallraff E, Deubzer B, Witke W, Gerisch G, Sackmann E. Biophys J. 1995; 68:1177. [PubMed: 7756537]
8. Verschueren H. J Cell Sci. 1985; 75:279. [PubMed: 3900106]
9. Braun D, Fromherz P. Appl Phys A. 1997; 65:341.
10. Braun D, Fromherz P. Phys Rev Lett. 1998; 81:5241.
11. Parthasarathy R, Groves JT. Cell Biochem Biophys. 2004; 41:391. [PubMed: 15509889]
12. Axelrod D. J Cell Biol. 1981; 89:141. [PubMed: 7014571]
13. Burmeister JS, Olivier LA, Reichert WM, Truskey GA. Biomaterials. 1998; 19:307. [PubMed: 9677147]
14. Burmeister JS, Truskey GA, Reichert WM. J Microsc. 1994; 173:39. [PubMed: 8120882]
15. Gingell D, Todd I, Bailey J. J Cell Biol. 1985; 100:1334. [PubMed: 2579959]
16. Hoover DK, Lee EJ, Yousaf MN. Langmuir: the ACS journal of surfaces and colloids. 2009; 25:2563. [PubMed: 19437680]
17. Giebel K, Bechinger C, Herminghaus S, Riedel M, Leiderer P, Weiland U, Bastmeyer M. Biophys J. 1999; 76:509. [PubMed: 9876164]
18. Peterson AW, Halter M, Tona A, Bhadriraju K, Plant AL. BMC Cell Biol. 2009; 10
19. Fragneto-Cusani G. Journal of Physics: Condensed Matter. 2001; 13
20. Krueger S. Current Opinion in Colloid & Interface Science. 2001; 6:111.
21. Majewski J, Kuhl TL, Gerstenberg MC, Israelachvili JN, Smith GS. The Journal of Physical Chemistry B. 1997; 101:3122.
22. Burgess I, Li M, Horswell SL, Szymanski G, Lipkowski J, Majewski J, Satija S. Biophys J. 2004; 86:1763. [PubMed: 14990503]
23. Fragneto G, Graner F, Charitat T, Dubos P, Bellet-Amalric E. Langmuir. 2000; 16:4581.
24. Koenig BW, Krueger S, Orts WJ, Majkrzak CF, Berk NF, Silverton JV, Gawrisch K. Langmuir. 1996; 12:1343.
25. Krueger S, Ankner JF, Satija SK, Majkrzak CF, Gurley D, Colombini M. Langmuir. 1995; 11:3218.
26. Doshi DA, Dattelbaum AM, Watkins EB, Brinker CJ, Swanson BI, Shreve AP, Parikh AN, Majewski J. Langmuir: the ACS journal of surfaces and colloids. 2005; 21:2865. [PubMed: 15779959]
27. Smith HL, Jablin MS, Vidyasagar A, Saiz J, Watkins E, Toomey R, Hurd AJ, Majewski J. Phys Rev Lett. 2009; 102
28. Dubey M, Jablin MS, Wang P, Mocko M, Majewski J. Eur Phys J Plus. 2011; 126:1.
29. Als-Nielsen J. Physica A: Statistical Mechanics and its Applications. 1986; 140:376.
30. Penfold J, Thomas RK. Journal of Physics: Condensed Matter. 1990; 2:1369.
31. Nelson A. Journal of Applied Crystallography. 2006; 39:273.

32. Smith HL, Hickey J, Jablin MS, Trujillo A, Freyer JP, Majewski J. Biophys J. 2010; 98:793. [PubMed: 20197032]
33. Pocivavsek L, Junghans A, Zebda N, Birukov K, Majewski J. American Journal of Physiology - Lung Cellular and Molecular Physiology. 2014; 306:L1. [PubMed: 24163142]
34. Kalb RG, Hockfield S. Neuroscience. 1990; 34:391. [PubMed: 2333149]
35. Birukov KG, Birukova AA, Dudek SM, Verin AD, Crow MT, Zhan X, DePaola N, Garcia JGN. Am J Respir Cell Mol Biol. 2002; 26:453. [PubMed: 11919082]
36. Birukova AA, Chatchavalvanich S, Rios A, Kawkitinarong K, Garcia JGN, Birukov KG. The American Journal of Pathology. 2006; 168:1749. [PubMed: 16651639]
37. Caro CG, Fitz-Gerald JM, Schroter RC. Proc R Soc Lond, B, Biol Sci. 1971; 177:109. [PubMed: 4396262]
38. White CR, Frangos JA. Philos Trans R Soc Lond, B, Biol Sci. 2007; 362:1459. [PubMed: 17569643]
39. Howard BV, Macarak EJ, Gunson D, Kefalides NA. Proc Natl Acad Sci USA. 1976; 73:2361. [PubMed: 59926]
40. Khoshnoodi J, Pedchenko V, Hudson BG. Microsc Res Tech. 2008; 71:357. [PubMed: 18219669]
41. Liliensiek SJ, Nealey P, Murphy CJ. Tissue Engineering Part A. 2009; 15:2643. [PubMed: 19207042]
42. Jablin MS, Zhernenkov M, Toperverg BP, Dubey M, Smith HL, Vidyasagar A, Toomey R, Hurd AJ, Majewski J. Phys Rev Lett. 2011; 106
43. Dudley AC. Cold Spring Harb Perspect Med. 2012; 2
44. Giaever I, Keese CR. Nature. 1993; 366:591. [PubMed: 8255299]
45. Tiruppathi C, Malik AB, Del Vecchio PJ, Keese CR, Giaever I. Proc Natl Acad Sci U S A. 1992; 89:7919. [PubMed: 1518814]
46. Bruinsma R, Behrisch A, Sackmann E. Phys Rev E Stat Phys Plasmas Fluids Relat Interdiscip Topics. 2000; 61:4253. [PubMed: 11088221]
47. Sackmann E, Bruinsma RF. Chem Phys Chem. 2002; 3:262. [PubMed: 12503172]
48. Alberts, B.; Bray, D.; Lewis, J.; Ra, M.; Roberts, K.; Watson, JD. Molecular Biology of the Cell. Garland Publishing; New York: 1994.
49. Boal, D. Mechanics of the Cell. Cambridge University Press; Cambridge: 2002.
50. Shiu, YT. Mechanical Forces on Cells. 3. CRC/Taylor-Francis; 2006.
51. Louis DN. Annual Review of Pathology: Mechanisms of Disease. 2006; 1:97.
52. Zong H, Verhaak RG, Canoll P. Expert Rev Mol Diagn. 2012; 12:383. [PubMed: 22616703]
53. Omuro A, DeAngelis LM. JAMA: the journal of the American Medical Association. 2013; 310:1842.
54. Miletic H, Niclou SP, Johansson M, Bjerkvig R. Expert Opin Ther Targets. 2009; 13:455. [PubMed: 19335067]
55. Nakada M, Nakada S, Demuth T, Tran NL, Hoelzinger DB, Berens ME. Cell Mol Life Sci. 2007; 64:458. [PubMed: 17260089]
56. Beadle C, Assanah MC, Monzo P, Vallee R, Rosenfeld SS, Canoll P. Mol Biol Cell. 2008; 19:3357. [PubMed: 18495866]
57. Gritsenko PG, Ilina O, Friedl P. The Journal of pathology. 2012; 226:185. [PubMed: 22006671]
58. Cuddapah VA, Robel S, Watkins S, Sontheimer H. Nature reviews Neuroscience. 2014; 15:455.
59. Bellail AC, Hunter SB, Brat DJ, Tan C, Van Meir EG. The international journal of biochemistry & cell biology. 2004; 36:1046. [PubMed: 15094120]
60. Viapiano, MS.; Lawler, SE. CNS Cancer: Models, Prognostic Factors and Targets. Van Meir, E., editor. Humana Press; New Jersey: 2009. p. 1219
61. Viapiano MS, Matthews RT. Trends Mol Med. 2006; 12:488. [PubMed: 16962376]
62. Heldin CH, Rubin K, Pietras K, Ostman A. Nat Rev Cancer. 2004; 4:806. [PubMed: 15510161]
63. Vargova L, Homola A, Zamecnik J, Tichy M, Benes V, Sykova E. Glia. 2003; 42:77. [PubMed: 12594739]
64. Qazi H, Shi ZD, Tarbell JM. PLoS One. 2011; 6:e20348. [PubMed: 21637818]

65. Jacobs VL, Valdes PA, Hickey WF, De Leo JA. ASN Neuro. 2011; 3:e00063. [PubMed: 21740400]

66. Glimelius B, Norling B, Westermark B, Wasteson A. J Cell Physiol. 1979; 98:527. [PubMed: 438297]

67. Glimelius B, Norling B, Westermark B, Wasteson A. Biochem J. 1978; 172:443. [PubMed: 687354]

68. Enegd B, King JA, Stylli S, Paradiso L, Kaye AH, Novak U. Neurosurgery. 2002; 50:1311. [PubMed: 12015850]

69. Sim H, Hu B, Viapiano MS. J Biol Chem. 2009; 284:26547. [PubMed: 19633295]

70. Newcomb, EW.; Zagzag, D. CNS Cancer: Models, Markers, Prognostic Factors, Targets and Therapeutic Approaches. Van Meir, EG., editor. Humana Press; NY: 2009. p. 227

71. Lauter-Pasyuk V, Lauter HJ, Gordeev GP, Müller-Buschbaum P, Toperverg BP, Jernenkov M, Petry W. Langmuir. 2003; 19:7783.

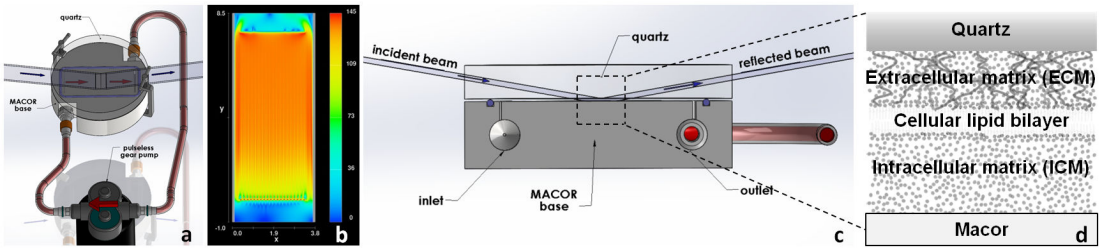

Figure 1. Schematic of the neutron scattering solid-liquid interface flow cell

(a) Schematic of the solid-liquid cell with clamping mechanism and gear pump. **(c)** Side view of the flow cell used for the experiments. **(b)** Results of hydrodynamic simulations of the fluid velocity distribution in the flow cell close to the quartz block, at the approximate live cell location. **(d)** Schematic of the live cells adhered to quartz wafer. After culturing the cells, the quartz substrate was clamped against a Macor disk with a 0.1–0.3 mm thick, subphase-filled gap created by an O-ring. The neutron beam penetrates the lateral face of the quartz substrate and is scattered from the solid-liquid interface.

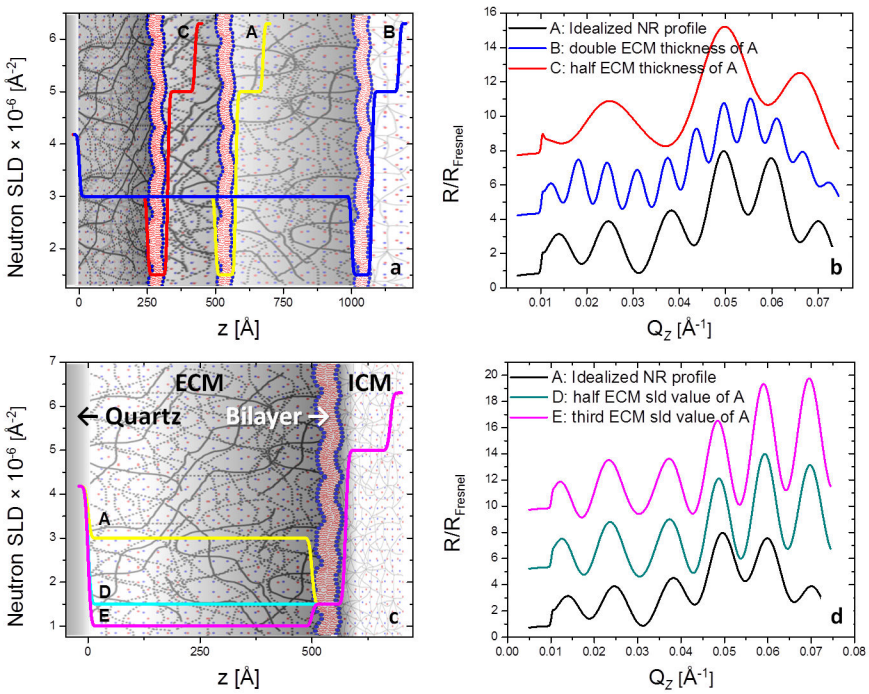

Figure 2. Simulated SLD distributions and corresponding calculated NR spectra

Left panel (**a**) – three SLD distributions corresponding to the same density of the scattering components but with the thickness of the extracellular cellular matrix (ECM) varied. Right panel (**b**) - simulated Fresnel divided NR spectra corresponding to the SLD profiles shown in (**a**). (**c**) - SLD distributions corresponding to the same thickness of the scattering components but with the amount of proteins in the ECM varied. (**d**) - calculated NR spectra corresponding to the SLD profiles shown in (**c**). The NR spectra are offset along y-axis for clarity. Parameters for the lipid bilayer (thickness, SLDs, roughness) of the cells and the intracellular matrix (ICM) have been kept constant.

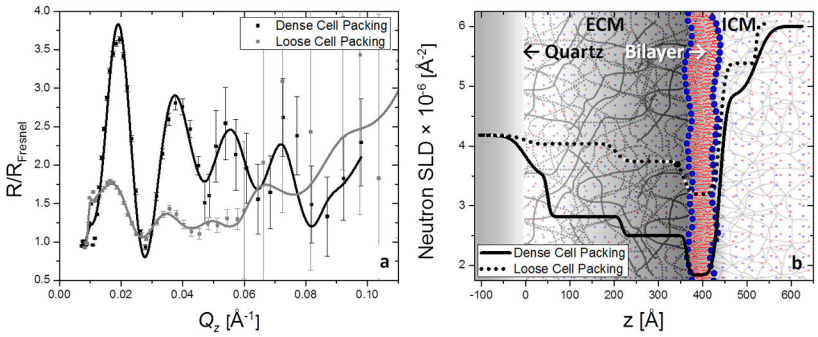

Figure 3. NR profiles and corresponding SLD distributions of mouse fibroblasts

Fresnel divided NR profiles **(a)** and corresponding SLD profiles **(b)** for high (***black***) and low (***gray***) cell surface densities. NR data are shown by closed squares, and error bars indicate 1 standard deviation (SD). The lower surface cell density is evident from the decreased scattering intensity (**a**) and the increased SLD in the membrane region (360–440 Å) and interior of the cell (440–600 Å) ***(b)***.

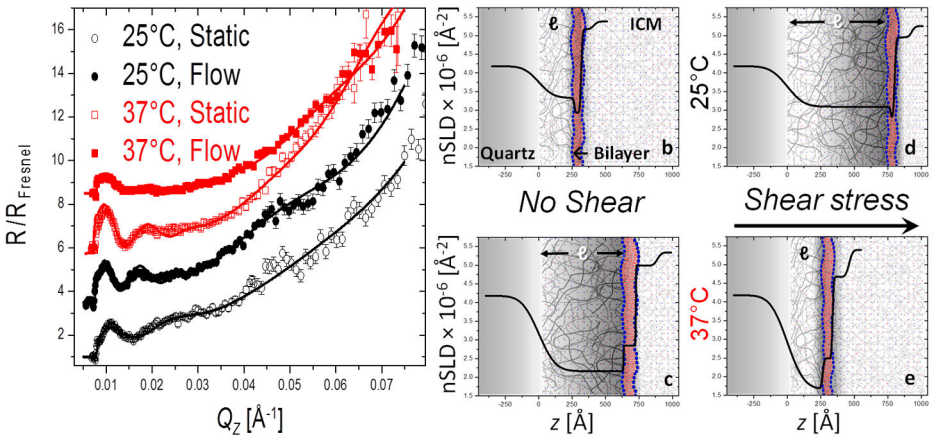

Figure 4. Differences in response to shear flow of healthy endothelial cells at ambient and physiological temperatures

Left (a): Fresnel-divided NR measurements (circles/squares with error bars) and corresponding best-fit models (solid lines) at the conditions studied. ***Black (open circles):*** 25° (Static), ***Black (closed circles):*** 25° Shear), ***Red (open squares):*** 37° (Static), ***Red (closed squares):*** 37° (Shear). The NR spectra are offset along y-axis for clarity. **Right (b-e):** SLD profiles obtained by fitting the data sets using a 3-box model (extracellular matrix – cell membrane – partial cell interior).

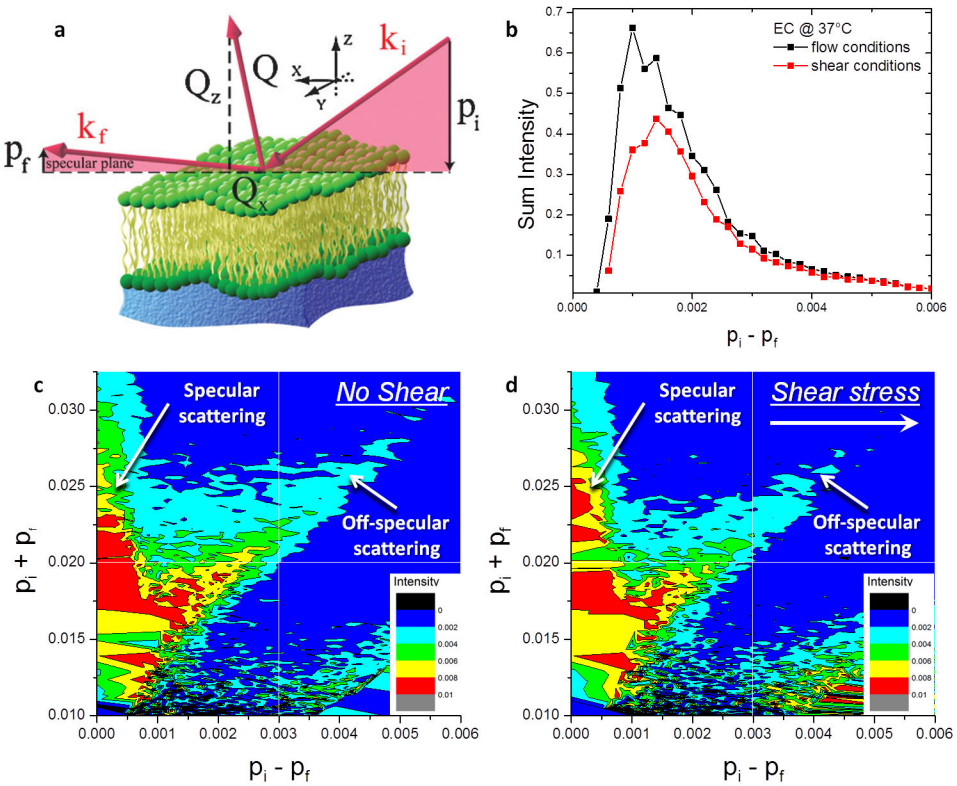

Figure 5. Off-specular data depicts changes in surface roughness

Data is shown as two-dimensional intensity maps as a function of p_i and p_f. (**a**) $p_i = 2\pi \sin \alpha_i/\lambda$ and $p_f = 2\pi \sin \alpha_f/\lambda$ are the components perpendicular to the sample surface of the incoming and outgoing neutron wave vectors, respectively [71]. The dominating intensity peak at $p_i - p_f = 0$ corresponds to the specular reflection Q_z. The off-specular (Yoneda scattering) is visible to the right from the specular line along picture's diagonal indicating the presence of surface and substrate roughness. **(b)** Comparison of the intensity distribution along the Yoneda peaks *vs.* $p_i - p_f$ of endothelial cells under static **(black)** and shear **(red)** conditions show decrease in scattering under shear stress. **(c)** and (**d**) show experimental two-dimensional intensity maps of endothelial cells at 37°C at static and shear conditions, respectively. The extension of the off-specular signal (right top corner) in (**c**) compared to (**d**) indicates more in-plane fluctuations at static conditions. The colors in all three panels correspond to the same intensity distributions pictured in a.

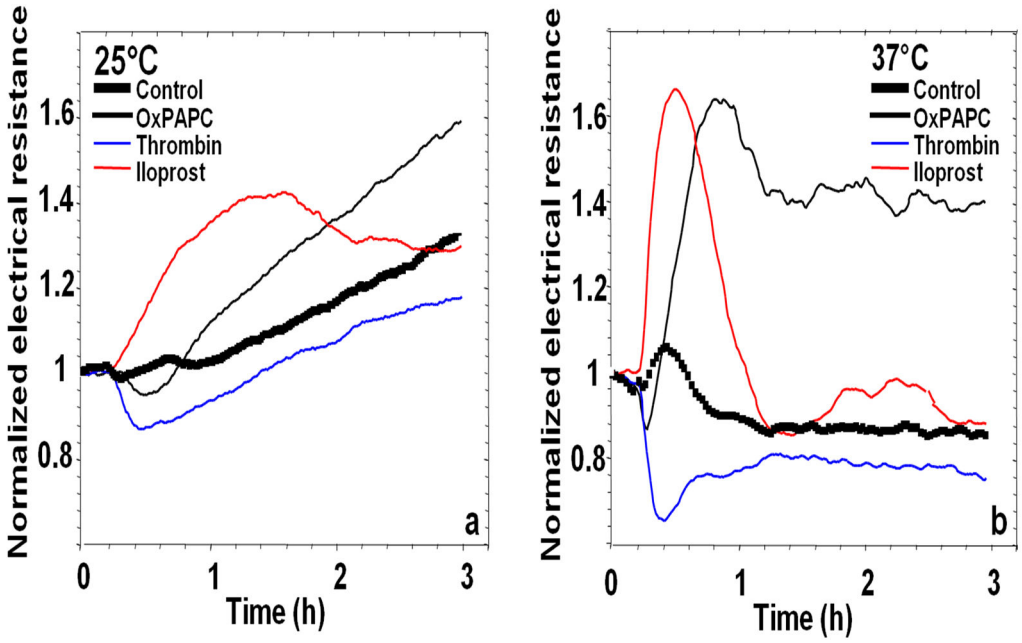

Figure 6. Temperature decrease suppresses endothelial cell permeability responses to agonists

Human pulmonary EC monolayers, at 25°C (**a**) and 37°C (**b**), grown on microelectrodes were stimulated with barrier-enhancing agonists OxPAPC (10 μg/ml) or iloprost (100 ng/ml), or cells were stimulated with barrier-disruptive agonist thrombin (1 U/ml). Trans-endothelial electrical resistance (TER) reflecting monolayer barrier property was measured over time. Sustained barrier enhancement by OxPAPC and transient barrier enhancement by iloprost was reflected by increases in TER. In contrast, thrombin-induced barrier compromise was reflected by rapid TER decline. The amplitude and rapidity of EC biological response to agonist stimulation observed at +37°C was significantly reduced at +25°C.

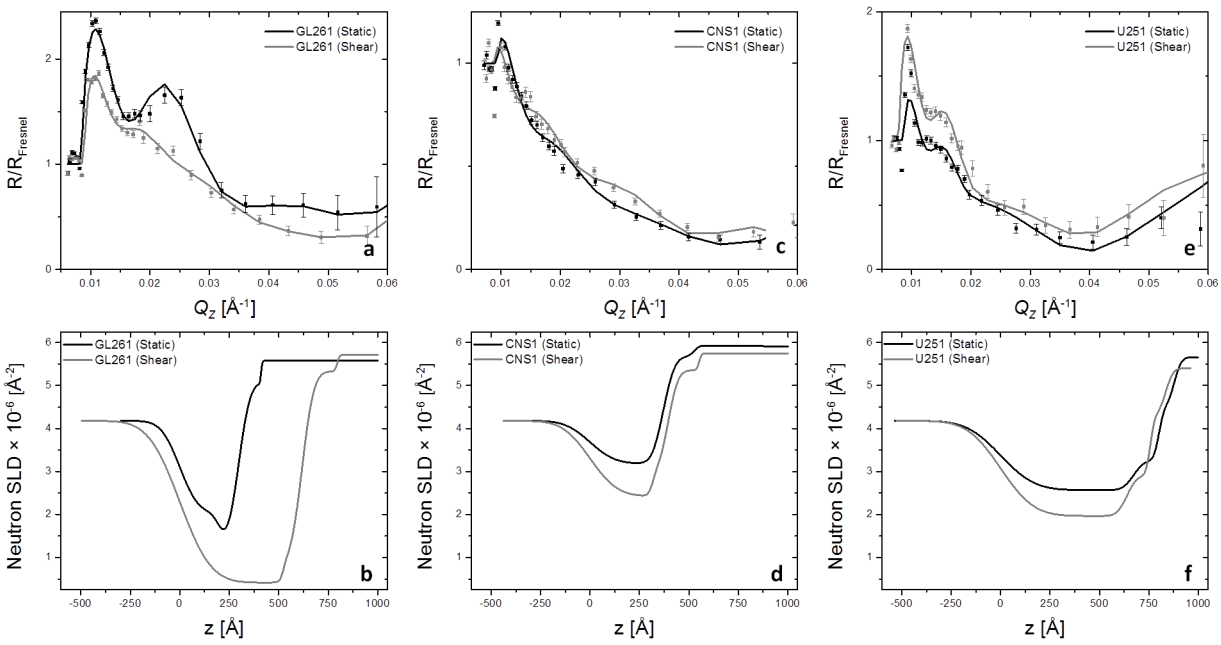

Figure 7. Differences in response to shear flow conditions of different GBM cell types

(**a, c, e):** Fresnel divided NR measurements (squares with error bars) and corresponding best-fit models (solid lines) of the three cell lines in contact with D_2O + 10% DMEM at 37°C. (**b, d, f):** SLD profiles obtained by fitting the data sets using a 3-box model (extracellular matrix – cell membrane – partial cell interior). ***(a, b):*** GL261, ***(c, d):*** CNS1, ***(e, f):*** U251.

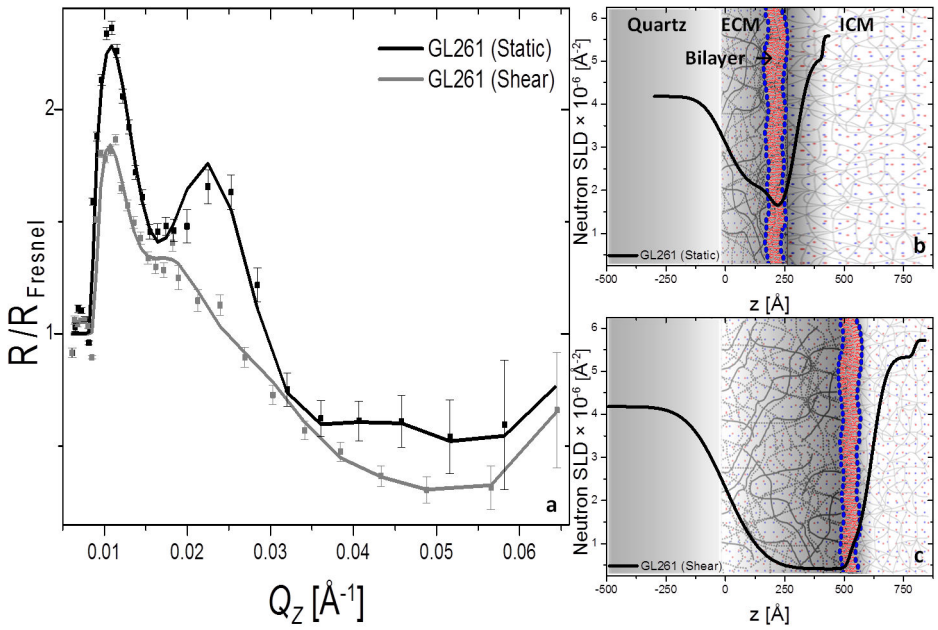

Figure 8. Behavior of GL261 cells under static and shear flow conditions

(a): Fresnel divided NR measurements (squares with error bars) and corresponding best-fit models (solid lines) of GL261 monolayer in contact with D_2O +10% DMEM at 37°C at static (***black***) and shear conditions (***gray***). (**b, c):** SLD profiles obtained by fitting the data shown in a using a 3-box model (extracellular matrix – cell membrane – partial cell interior) at static (**b**) and shear conditions (**c**).

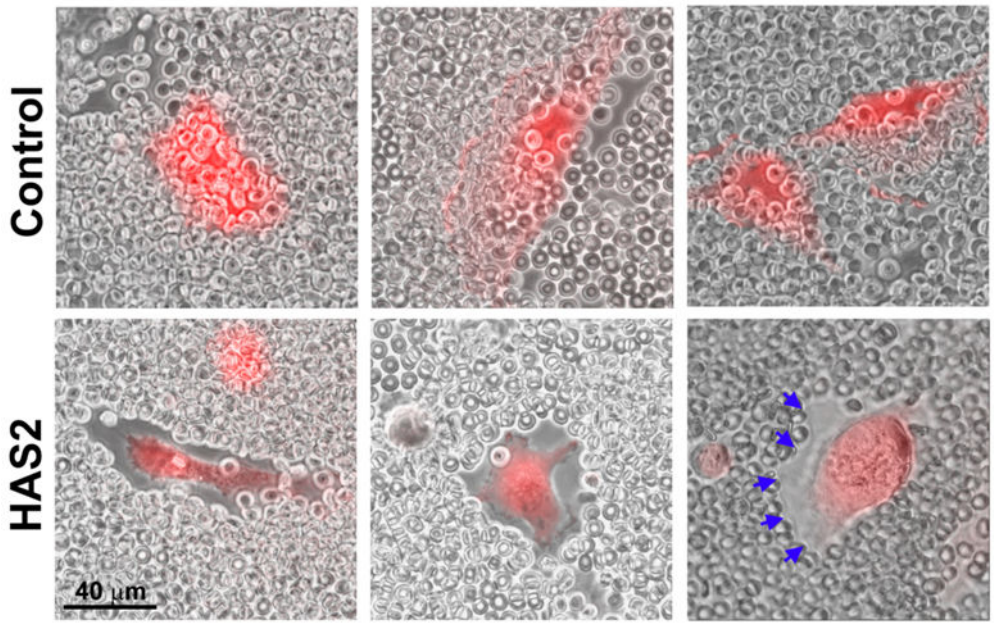

Figure 9.

Cells transfected with HAS2 gene produces large pericellular coats of HA. U251 glioma cells expressing red fluorescent protein were transfected with a plasmid carrying the HA-synthase enzyme HAS2 or a negative control. Two days after transfection, live cells were incubated with fixed erythrocytes, which cannot permeate the HA mesh, and imaged by fluorescence (to reveal the cytoplasm) and phase-contrast (to reveal their pericellular coats, marked by arrows). Bar: 40 μm. This research was originally published in: Sim *et al*. Reduced expression of the hyaluronan and proteoglycan link proteins in malignant gliomas. *J Biol Chem* (2009) 284:26547. (c) The American Society for Biochemistry and Molecular Biology.

Table I

Glioblastoma cell lines analyzed by neutron reflectometry

Cell line	Species	Origen	Invasive properties	Morphology	References
U251MG	Human	Established from a 75-year old patient by passage in culture. Exhibit amoeboid morphology with large lamellipodia	Very limited infiltration in the brain, restricted to local dispersion close to the tumor. Spread along the internal surface of the meninges is sometimes present	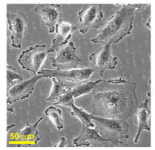	66, 67
GL261	Mouse	Chemically induced by intracerebral implantation of methylcholantrene pellets in C57Bl6 mice. Exhibit typical fibroblastic morphology	Local dispersion away from the tumor core, resulting in irregular tumor borders. Most invasion is local around the tumor but dispersion of individual cells and groups of cells can be seen along blood vessels	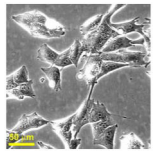	68
CNS1	Rat	Chemically induced by repeated intracranial injection of methylnitrosourea in Lewis rats. Appear as small, highly motile fibroblasts	Highly invasive cells, able to disperse long distances away from the tumor core. Cells invade brain tissue along perivascular and periventricular spaces. Invasion of single cells along white matter can reach the opposite brain hemisphere	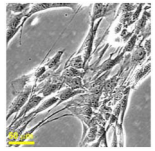	66, 69